

http://topex.ucsd.edu/gmtsar/tar/GMTSAR_2ND_TEX.pdf

GMTSAR:
An InSAR Processing System
Based on Generic Mapping Tools
(Second Edition)

David Sandwell* Rob Mellors[†] Xiaopeng Tong^{*‡}
Xiaohua Xu* Matt Wei[§] Paul Wessel[¶]

May 1, 2011; Revised: June 1, 2016

Contents

1 Introduction	5
1.1 Objectives and limitations of GMTSAR	5
1.2 Algorithms: SAR, InSAR, and the need for precise orbits	6
1.2.1 Proper focus	7
1.2.2 Transformation from geographic to radar coordinates	8
1.2.3 Image alignment	9
1.2.4 Flattening interferogram - no trend removal	10
2 Software	11
2.1 Standard Products	11
2.2 Software Design	12
3 Processing Examples	14
3.1 Two-pass processing	15
3.2 Stacking for time series	18
3.3 ScanSAR Interferometry	26
4 Problems	32
A Principles of Synthetic Aperture Radar	33
A.1 Introduction	33
A.2 Fraunhofer diffraction	34
A.3 2-D Aperture	37
A.4 Range resolution (end view)	38
A.5 Azimuth resolution (top view)	39
A.6 Range and Azimuth Resolution of ERS SAR	40
A.7 Pulse repetition frequency	40
A.8 Other constraints on the PRF	40
A.9 Problems	42
B SAR Image Formation	44
B.1 Overview of the range-doppler algorithm	44
B.2 Processing on board the satellite	44
B.3 Digital SAR processing	45
B.4 Range compression	49
B.5 Azimuth compression	51
B.6 Example with ALOS L-band orbit	58
B.7 Problems	61
C InSAR	62
C.1 Forming an interferogram	62
C.2 Contributions to Phase	63
C.3 Phase due to earth curvature	64
C.4 Look angle and incidence angle for a spherical earth	65
C.5 Critical baseline	67
C.6 Persistent point scatterer and critical baseline	68
C.7 Phase due to topography	69
C.8 Altitude of ambiguity	70
C.9 Phase due to earth curvature and topography – exact formula	70
C.10 Problems	74
D ScanSAR Processing and Interferometry	75
D.1 Problems	80
E Sentinel TOPS-mode processing and interferometry	81
E.1 Introduction	81
E.2 Traditional Image Alignment Fails with TOPS-Mode Data	83
E.3 Geometric Image Registration	84
E.4 Enhanced Spectral Diversity	86
E.5 Elevation Antenna Pattern (EAP) Correction (IPF version change)	87
E.6 Examples of TOPS Interferogram processing	87
E.7 Processing setup and commands:	97
E.8 Problems	99
F Geolocation accuracy for Pinon corner reflectors	100
G Installation of GMTSAR	107

forming interferogram

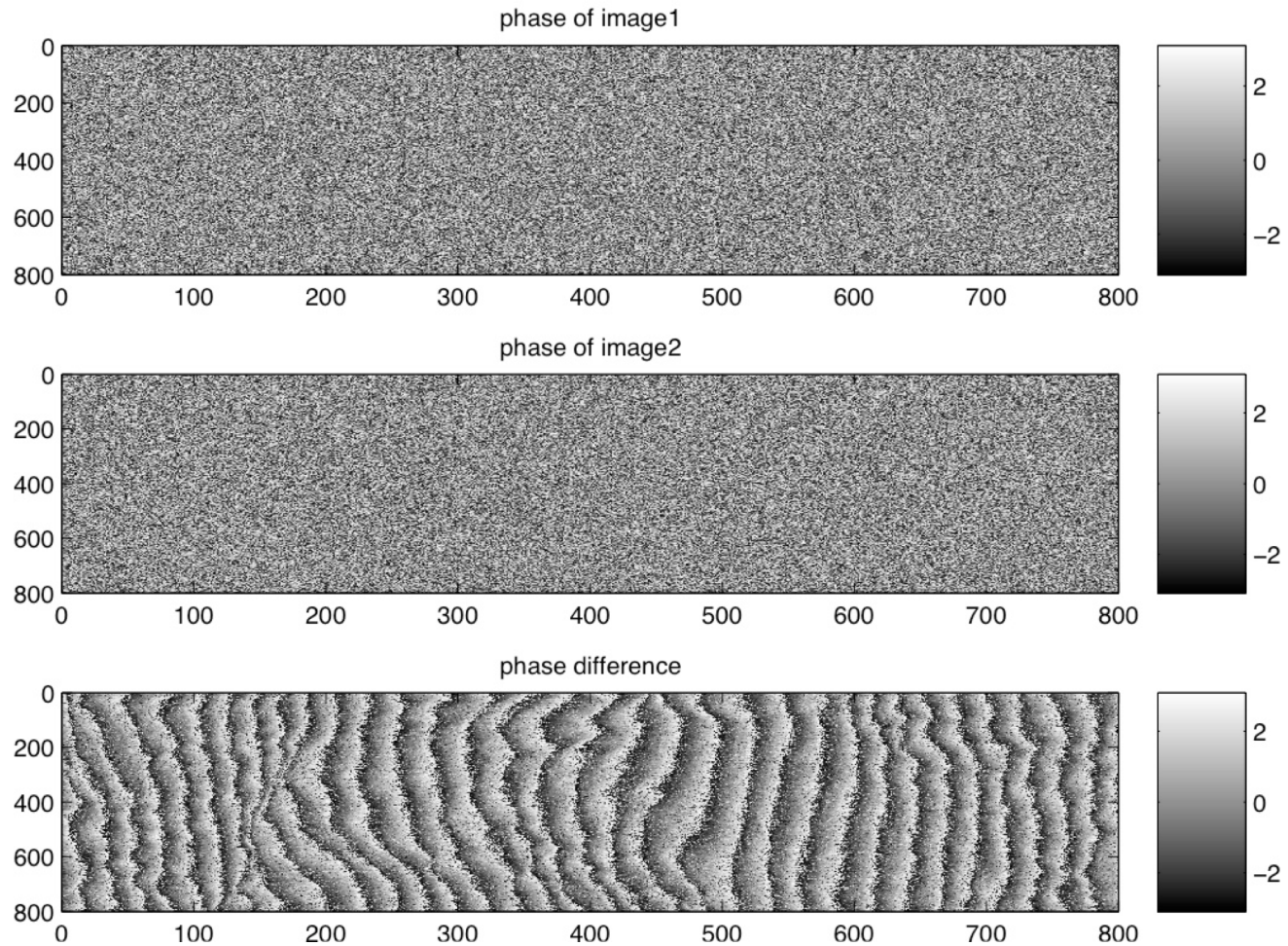
$$C(\mathbf{x}) = A(\mathbf{x})e^{i\phi(\mathbf{x})} \quad (\text{C1})$$

where $\mathbf{x} = (\rho, a)$ is the position vector consisting of range ρ and azimuth a . Their product is

$$C_2 C_1^* = A_1 A_2 e^{i(\phi_2 - \phi_1)} = R(\mathbf{x}) + iI(\mathbf{x}). \quad (\text{C2})$$

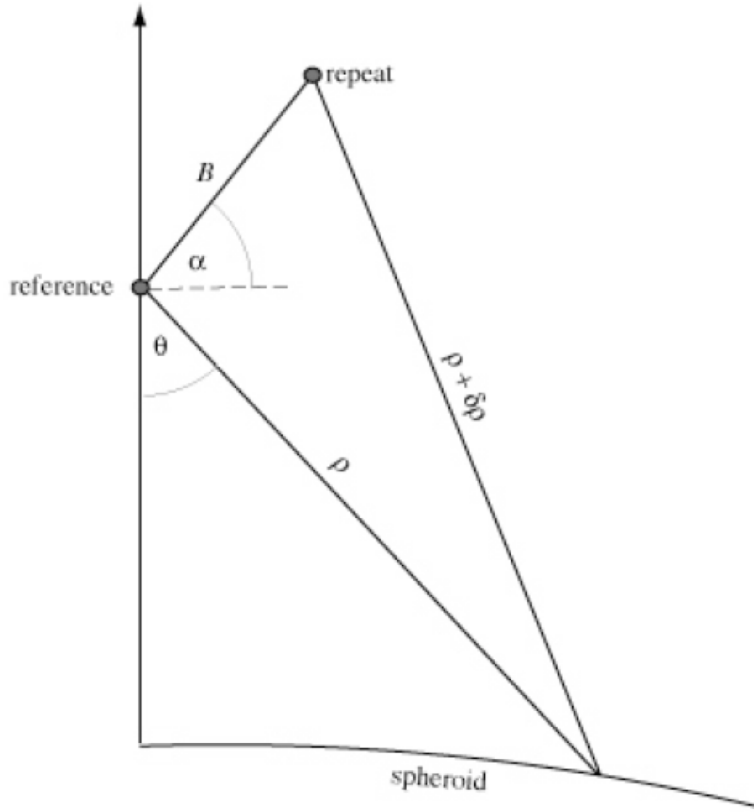
The phase of the interferogram is extracted in the usual way.

$$(\phi_2 - \phi_1) = \tan^{-1}\left(\frac{I}{R}\right) \quad (\text{C3})$$



phase =

**earth curvature (almost a plane, known) +
topographic phase (broad spectrum) +
surface deformation (broad spectrum, unknown) +
orbit error (almost a plane, largely known) +
ionosphere delay (a plane or 40-km wavelength waves) +
troposphere delay (power law, unknown) +
phase noise (white spectrum, unknown)**



$$(\rho + \delta\rho)^2 = \rho^2 + B^2 - 2\rho B \sin(\theta - \alpha) \quad (C7)$$

Next we make two standard approximations that are useful for introducing interferometric concepts but are unnecessary and also lead to inaccurate results. First we assume $\delta\rho \ll \rho$ so we have

$$\delta\rho = \frac{B^2}{2\rho} - B \sin(\theta - \alpha). \quad (C8)$$

Furthermore since $B \ll \rho$ the parallel ray approximation yields.

$$\phi = \frac{-4\pi}{\lambda} B \sin(\theta - \alpha) \quad (C9)$$

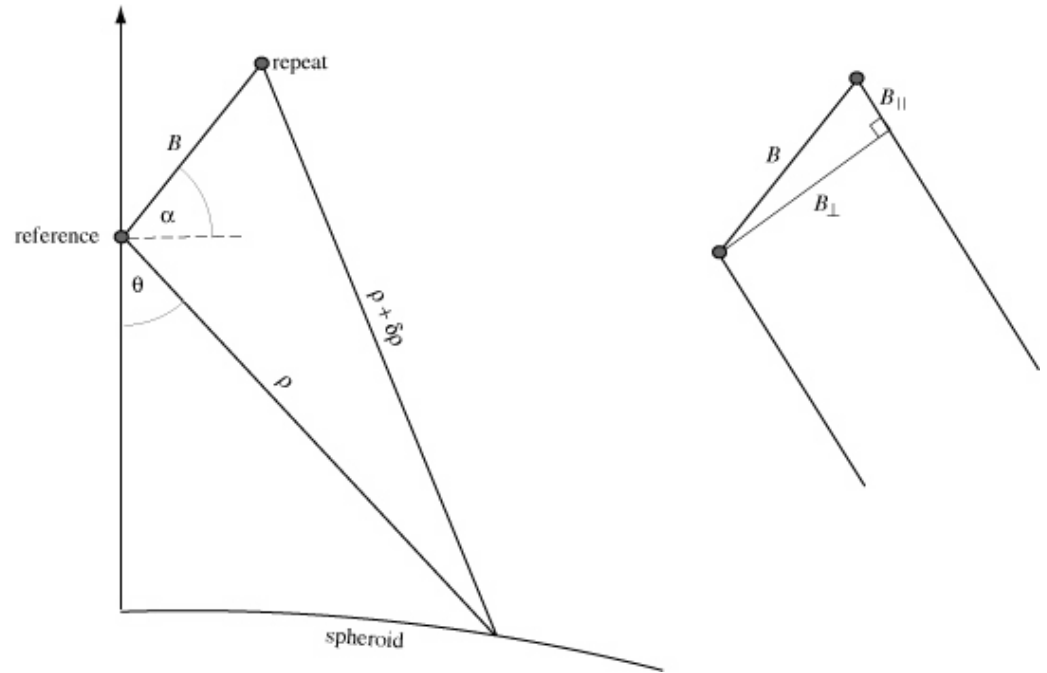
The phase difference depends on the parallel component of the baseline. The derivative of the phase with respect to range is

$$\frac{\partial\phi}{\partial\rho} = \frac{-4\pi}{\lambda} B \cos(\theta - \alpha) \frac{\partial\theta}{\partial\rho} \quad (C10)$$

Perpendicular baseline
MATTERS!

$$B_{\parallel} = B \sin(\theta - \alpha)$$

$$B_{\perp} = B \cos(\theta - \alpha)$$



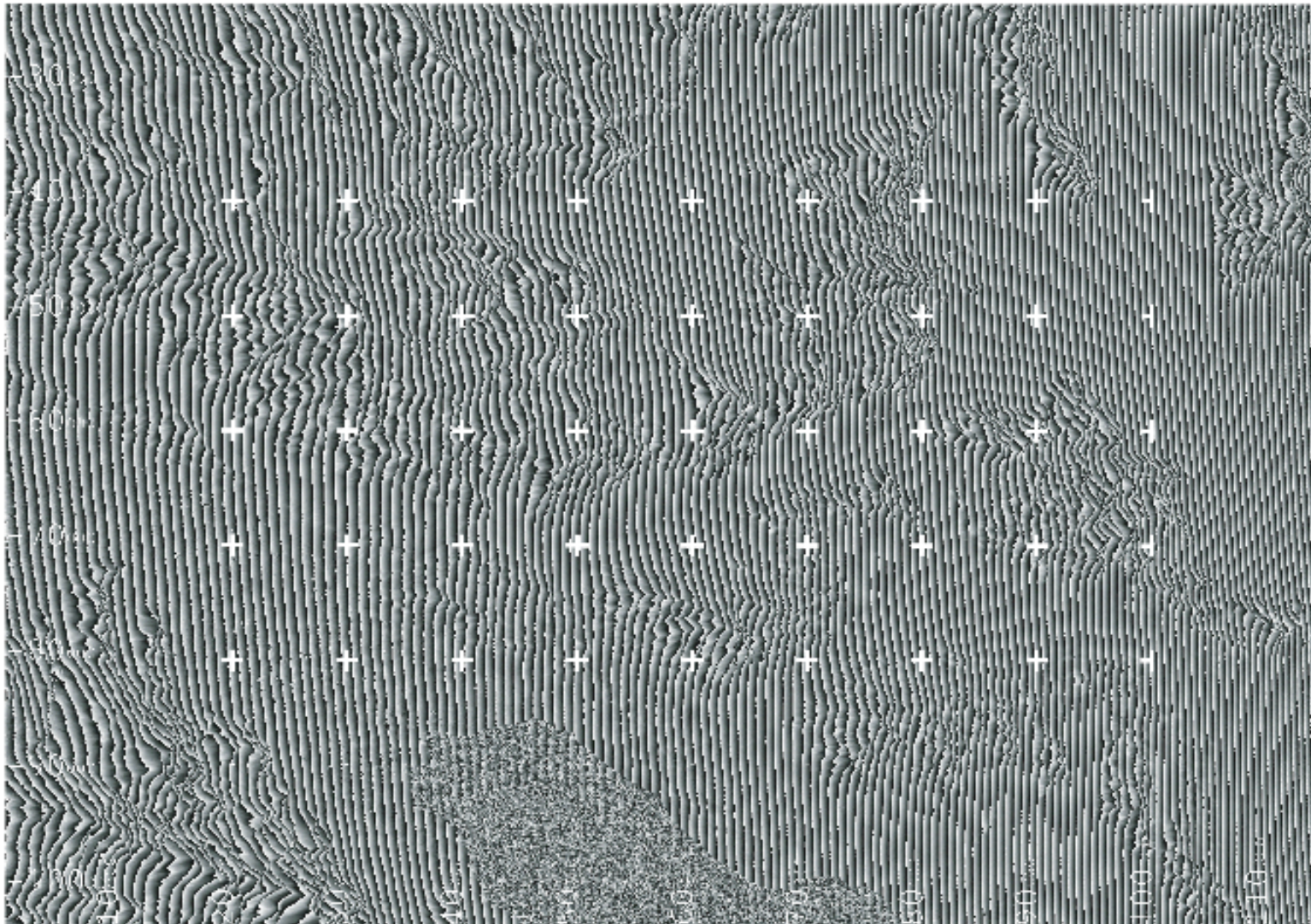
$$\frac{\partial \phi}{\partial \rho} = \frac{-4\pi B \cos(\theta - \alpha)}{\lambda \rho \sin \theta} \left(\cos \theta - \frac{\rho}{b} \right)$$

phase due to curved earth

$$(\phi - \phi_e) \cong \frac{-4\pi r_e B \cos(\theta - \alpha)}{\lambda \rho b \sin \theta} (r - r_e)$$

phase due to topography

total phase



3) This is an interferogram made from ERS SAR data. One fringe represents 2π phase change between the reference and repeat SAR acquisition. Count the fringes across the image and calculate the perpendicular baseline. You will need the look angle from the previous problem. The total change in slant range across the image is 50 km. Why does the fringe rate vary slightly across the image?

Phase from curved Earth

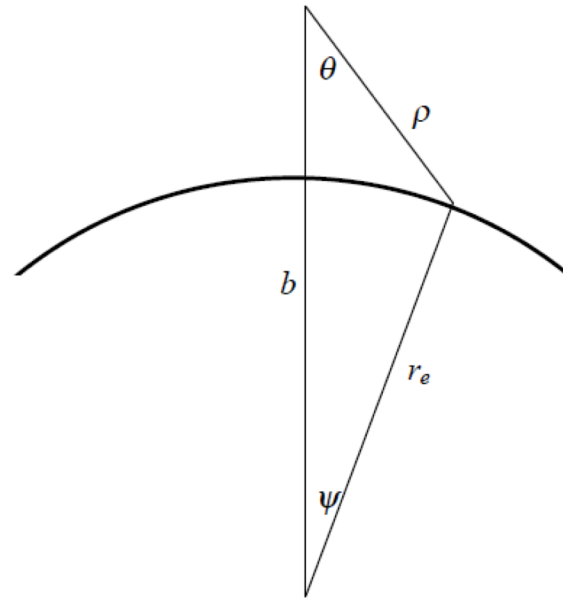


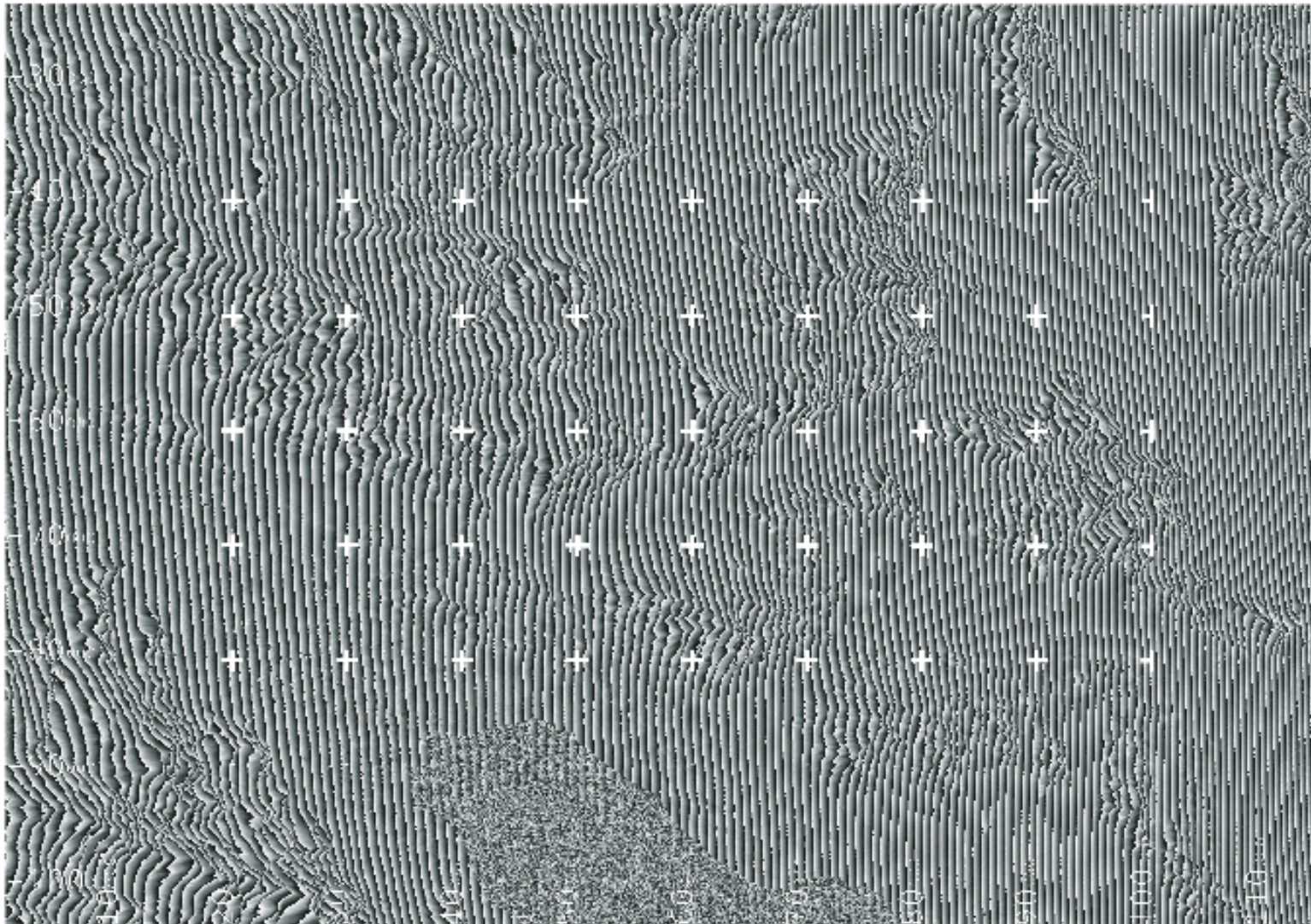
Figure C3 Triangle formed by the range ρ , radius of the earth r_e and spacecraft height b .

Using the Law of cosines one finds

$$\eta = \cos \theta = \frac{(b^2 + \rho^2 - r_e^2)}{2\rho b} \quad (\text{C12})$$

$$\frac{\partial \phi}{\partial \rho} = \frac{-4\pi B \cos(\theta - \alpha)}{\lambda \rho \sin \theta} \left(\cos \theta - \frac{\rho}{b} \right) \quad ($$

total phase



3) This is an interferogram made from ERS SAR data. One fringe represents 2π phase change between the reference and repeat SAR acquisition. Count the fringes across the image and calculate the perpendicular baseline. You will need the look angle from the previous problem. The total change in slant range across the image is 50 km. Why does the fringe rate vary slightly across the image?

Critical Baseline

$$\frac{\partial \phi}{\partial \rho} = \frac{-4\pi B_{\perp}}{\lambda \rho} \frac{\cos \theta}{\sin \theta} < \frac{2\pi}{\Delta \rho}$$

$$B_c = \frac{\lambda \rho}{C \tau} \tan \theta \quad . \quad (C16)$$

For the parameters of the ERS satellite the critical baseline is 1100 m (Tabel 1). For topographic recovery, a baseline of about 1/4 critical is optimal. Of course for change detection, a zero baseline is optimal but not usually available.

Table 1. Comparison of critical baseline

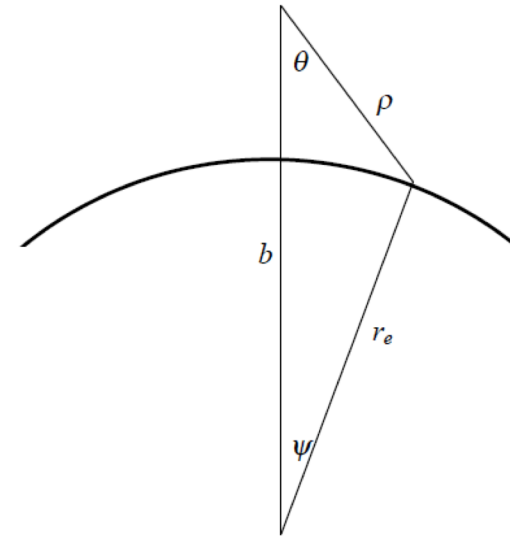
look angle	23°	34°	41°
ERS/ENVISAT 16 MHz	1.1 km	2.0	2.9
ALOS FBD 14 MHz	3.6	6.5	9.6
ALOS FBS 28 MHz	7.3	13.1	18.6

ERS/ENVISAT - altitude = 790 km, wavelength = 56 mm

ALOS - altitude = 700 km, wavelength = 236 mm

Shaded area is most common mode for interferometry.

Phase from topography



$$\frac{\partial \phi}{\partial r}(r_e) = \frac{-4\pi r_e B \cos(\theta_e - \alpha)}{\lambda \rho b \sin \theta_e}$$

where θ_e is the look angle to the spheroid (C12).

into elevation as a function of range is

$$(r - r_e) = \frac{-\lambda \rho b \sin \theta_e}{4\pi r_e B \cos(\theta_e - \alpha)} (\phi - \phi_e)$$

$$h_a = \frac{\lambda \rho \sin \theta_e}{2B_{\perp}}$$

(C21)

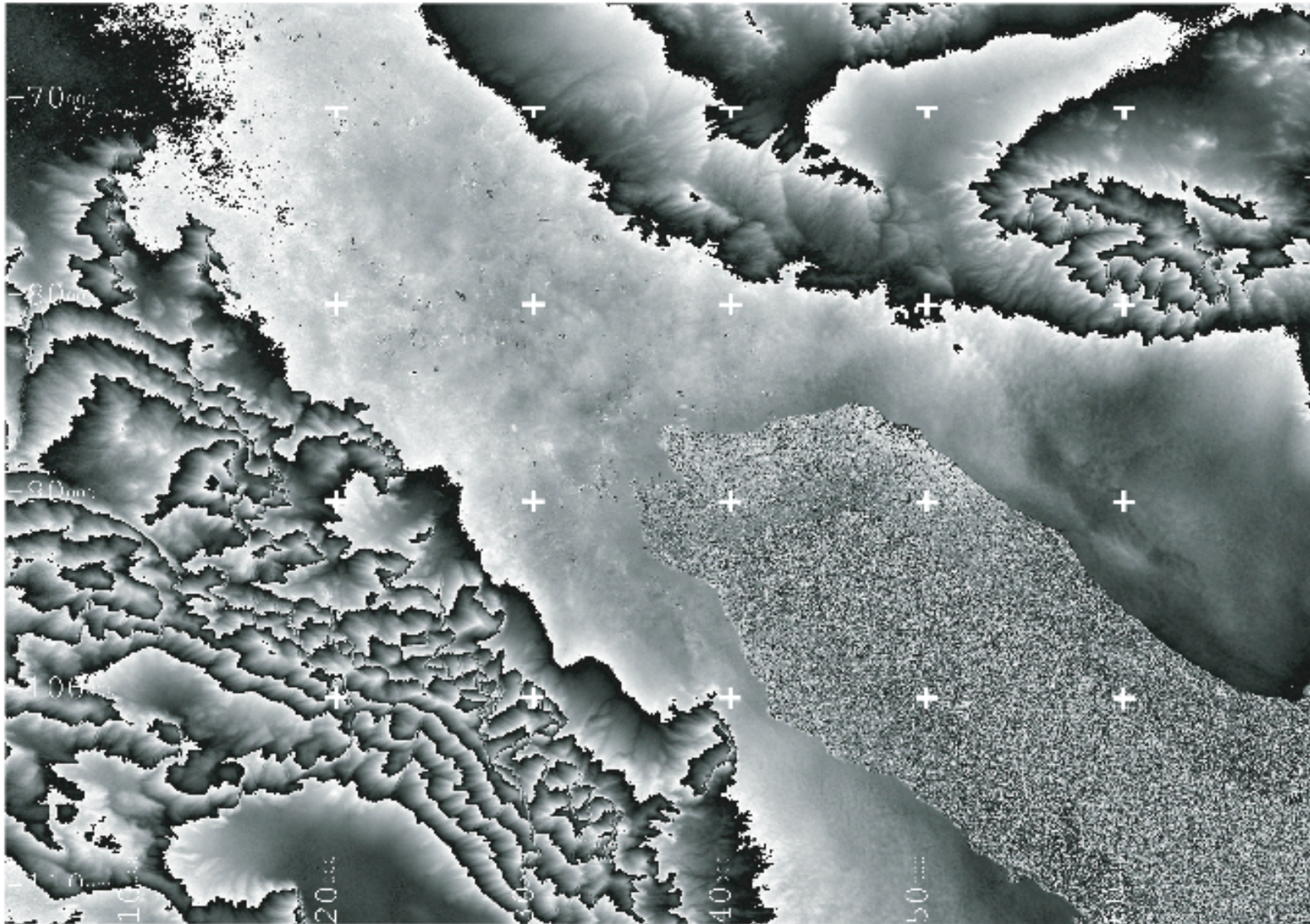
For the case of ERS with a perpendicular baseline of 100 m, this altitude of ambiguity is about 90 m. For change detection, a higher number is better.

Figure C3 Triangle formed by the range ρ , radius of the earth r_e and spacecraft height b .

Using the Law of cosines one finds

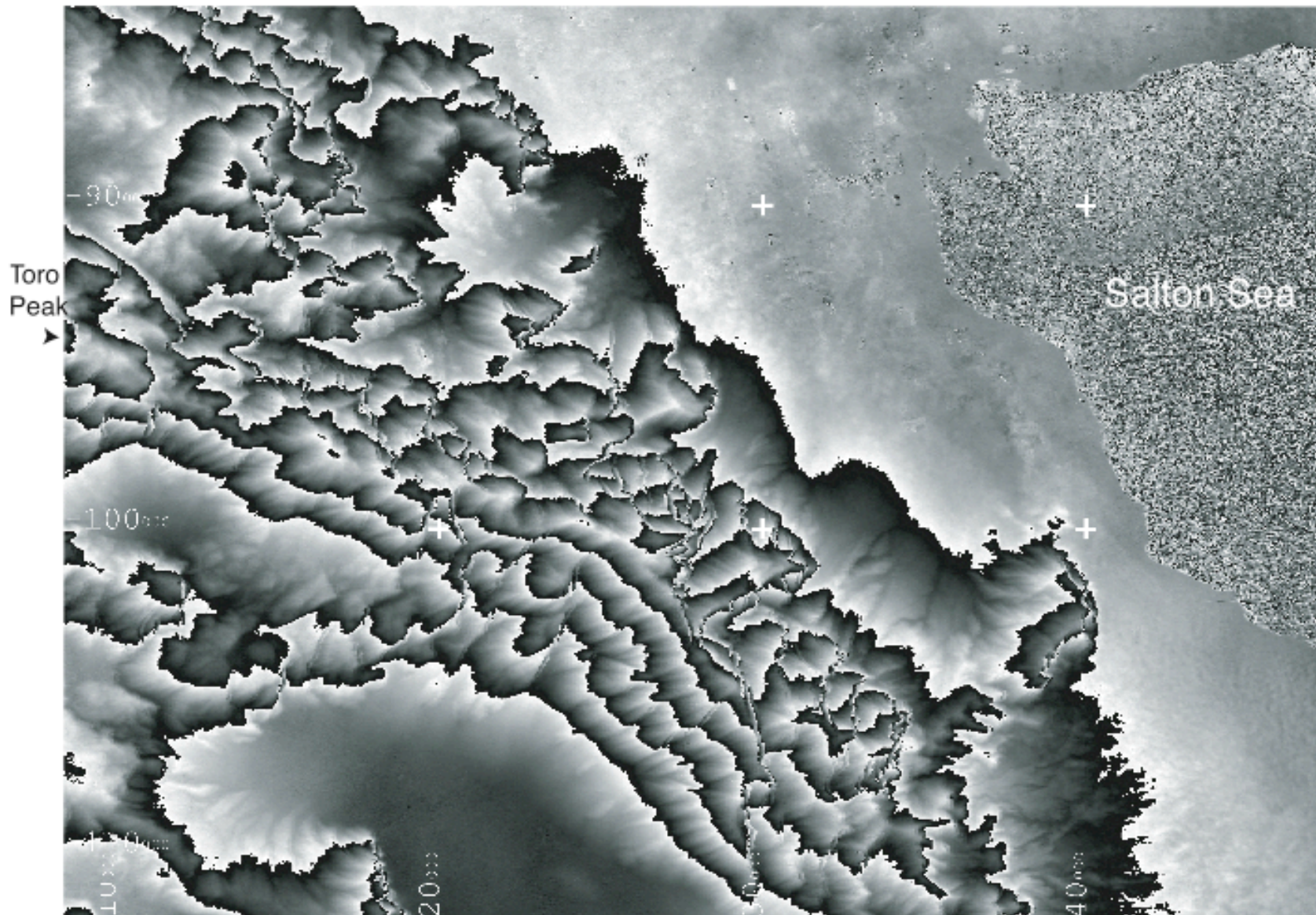
$$\eta = \cos \theta = \frac{(b^2 + \rho^2 - r_e^2)}{2\rho b} \quad (C1)$$

phase minus spherical earth



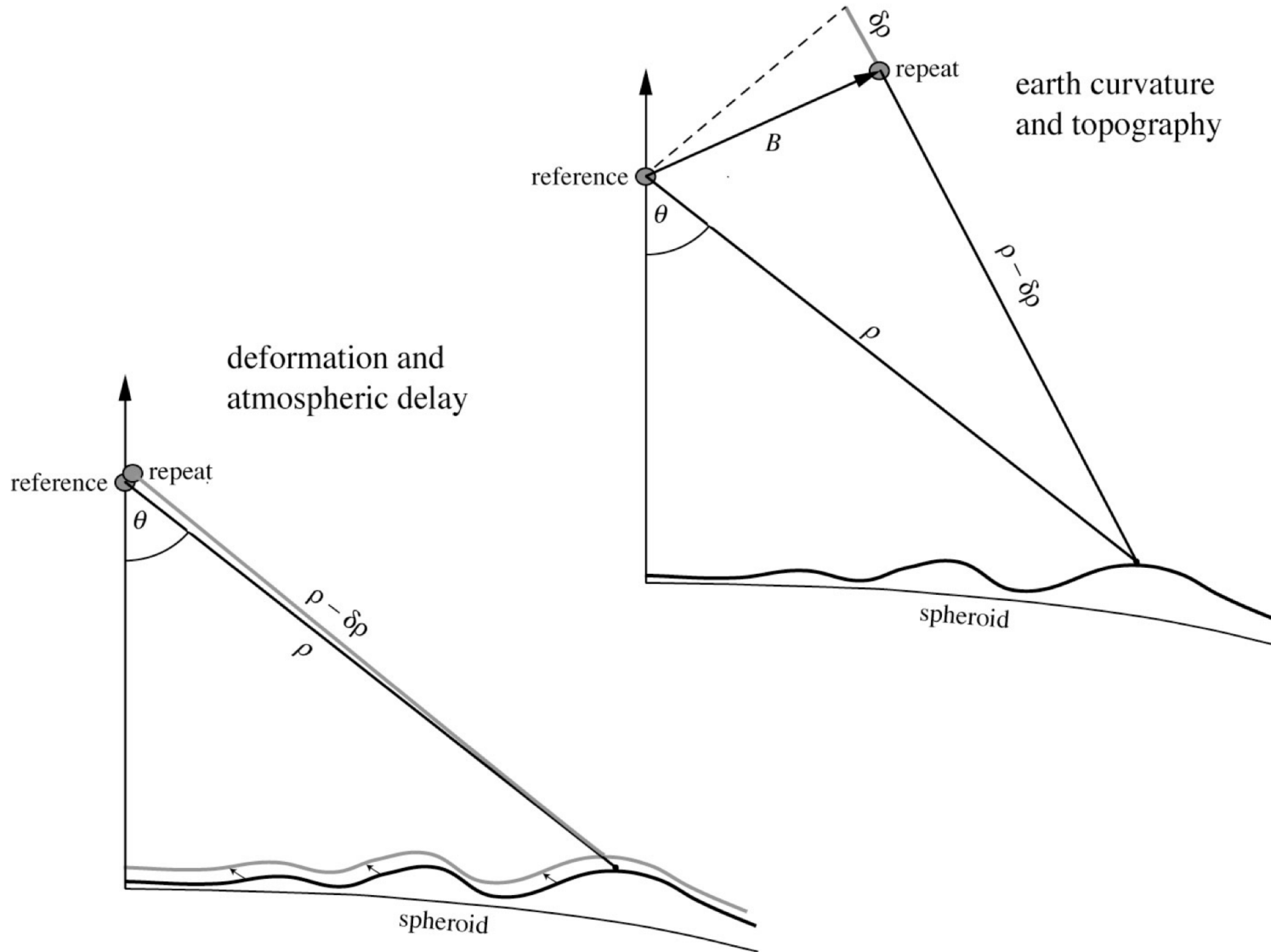
4) Interferogram with fringes due to geometry and Earth curvature removed. What are the cause(s) of the residual fringes? Why is the phase along the shoreline of the Salton Sea not exactly constant? (there are several possibilities).

How high is Toro Peak?

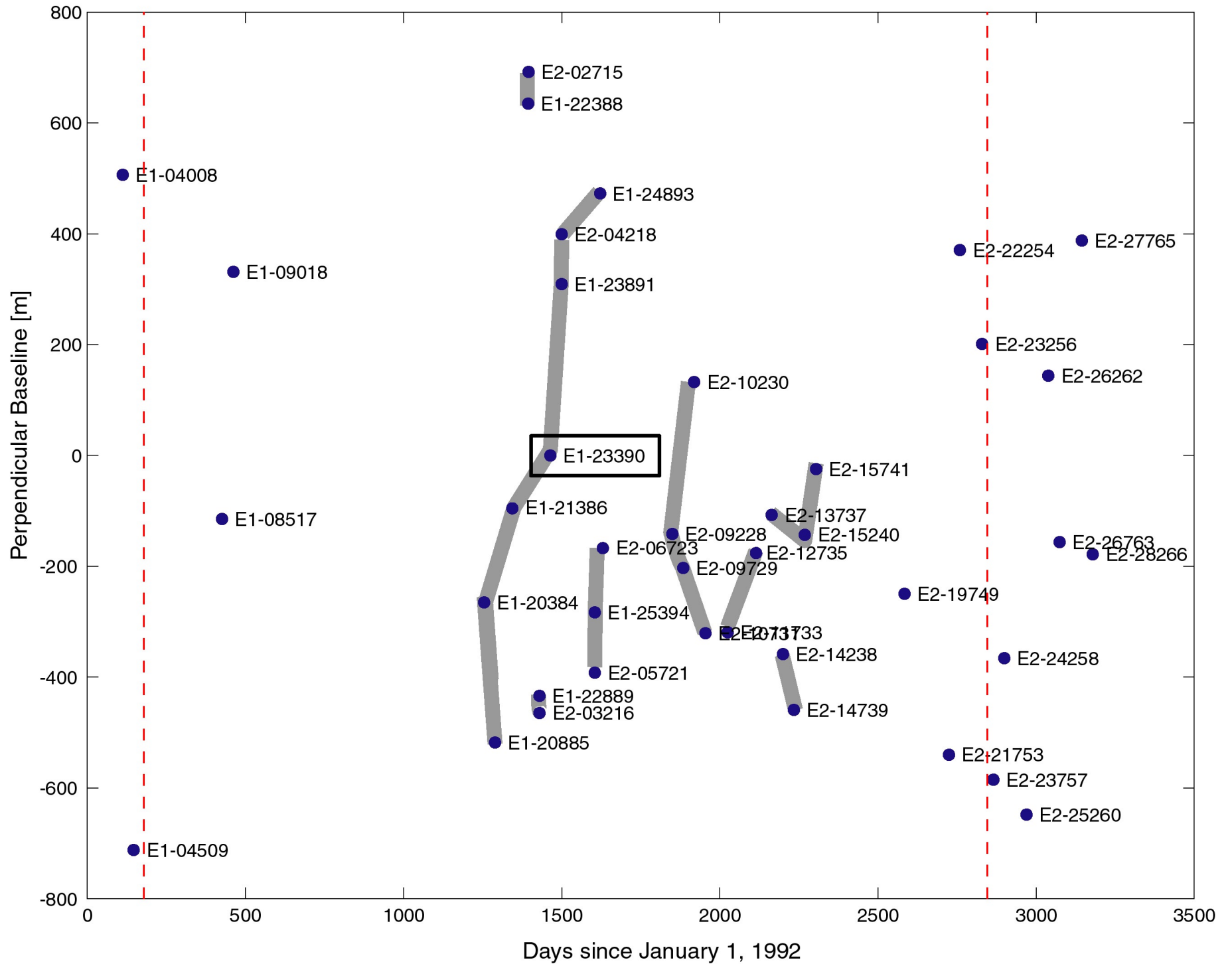


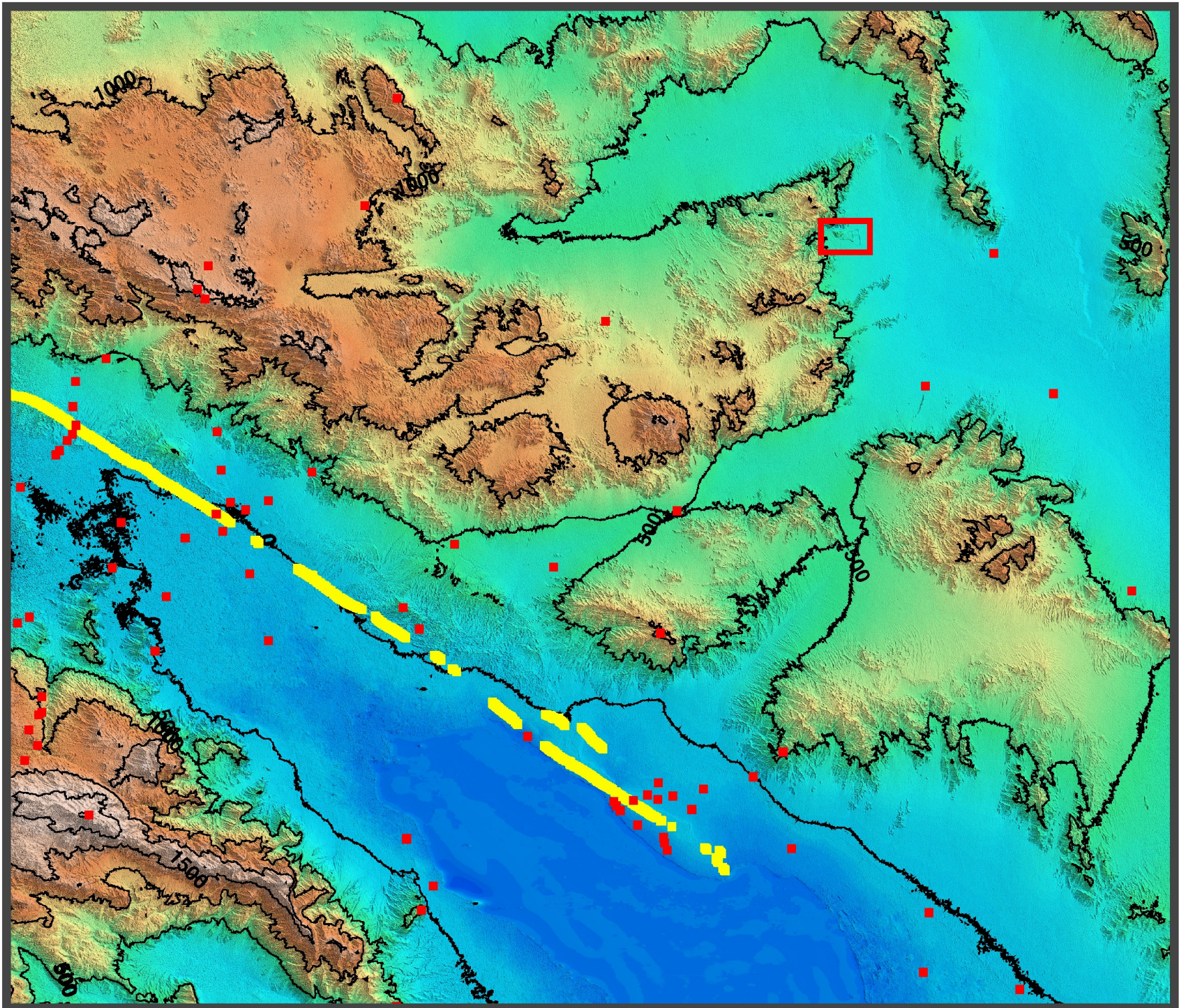
5) This is a zoom of the previous interferogram. Estimate the height difference between Toro Peak and the Salton Sea. Identify areas of layover?

deformation and topography

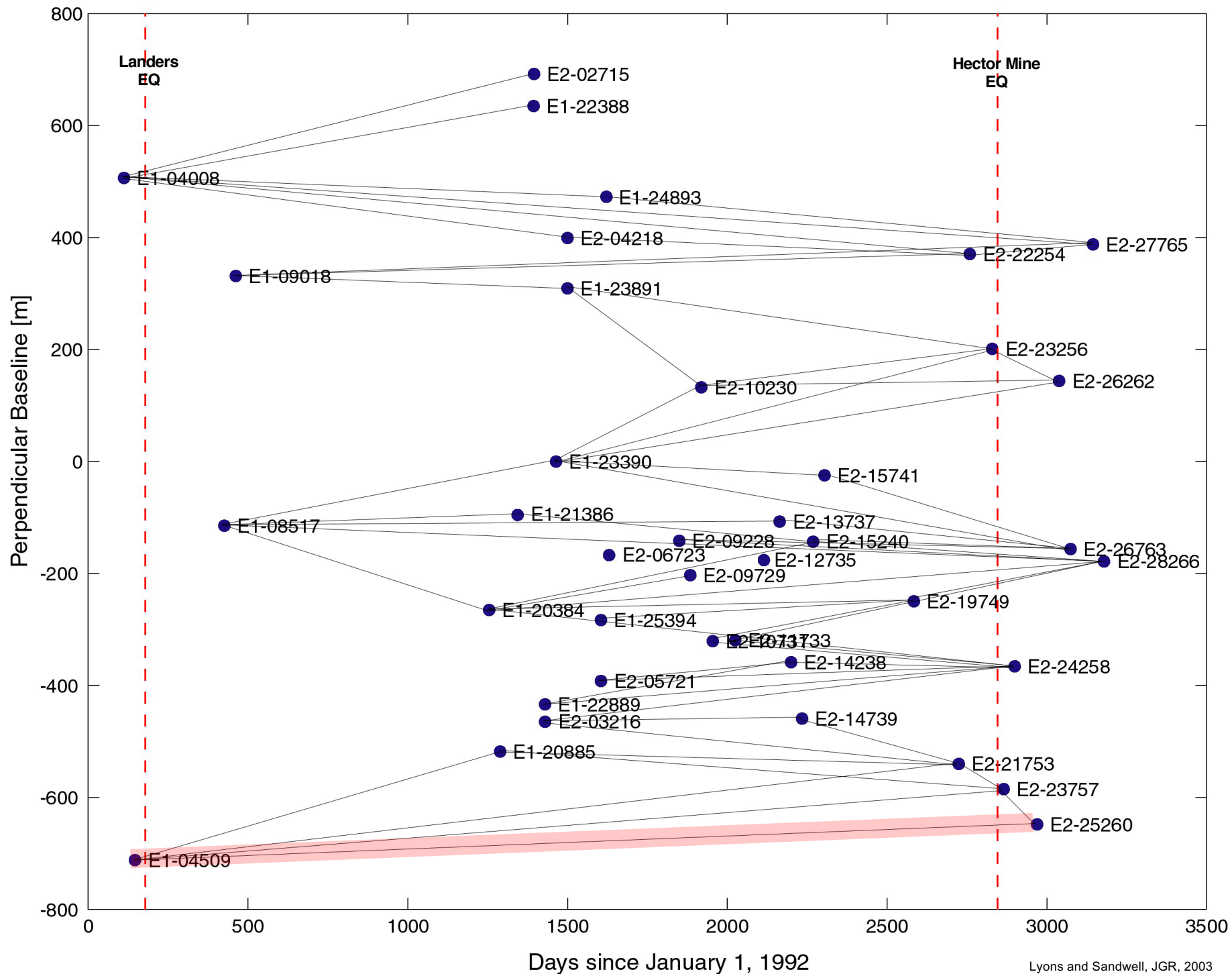


Topographic Pairs

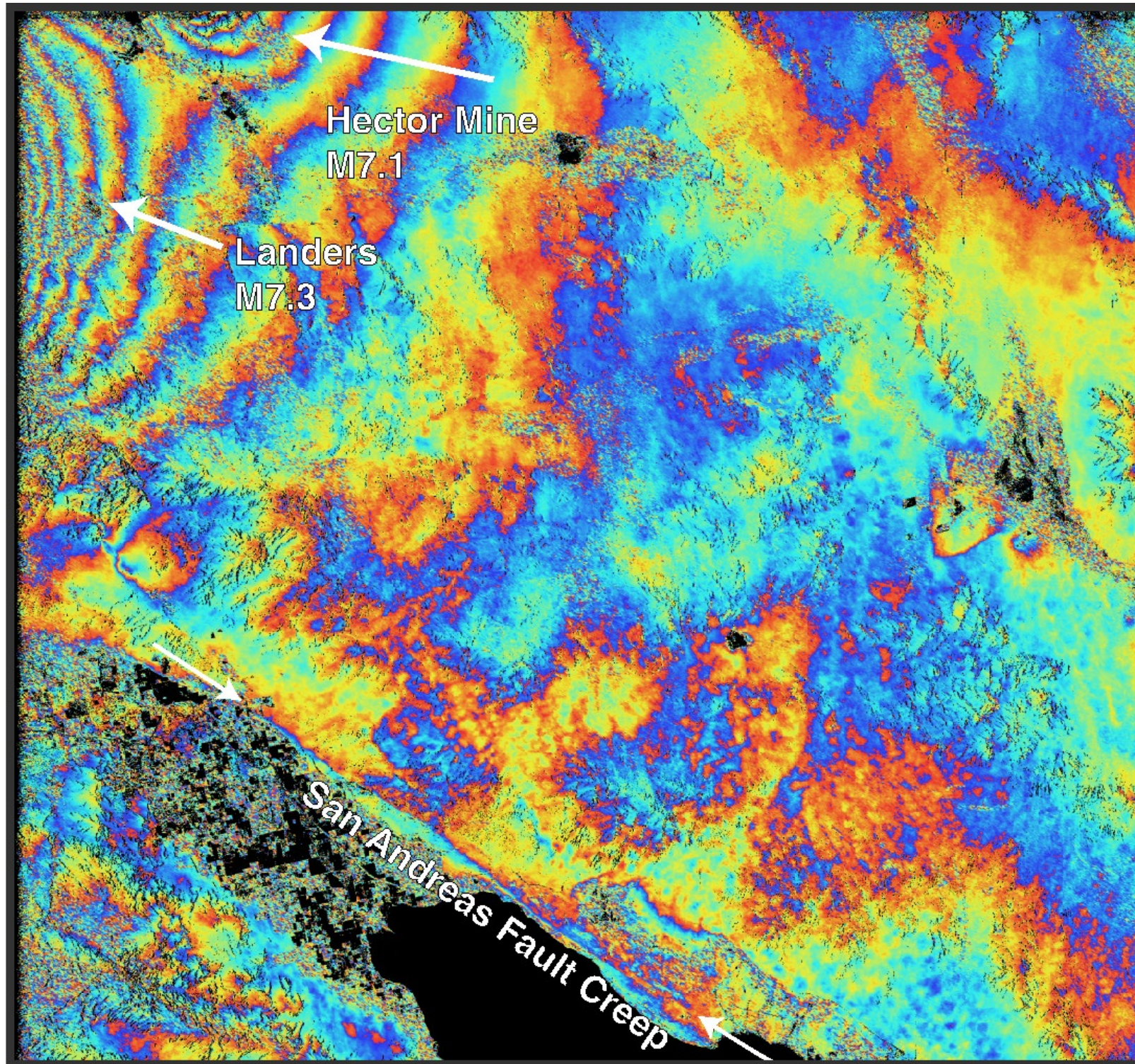




Change Pairs

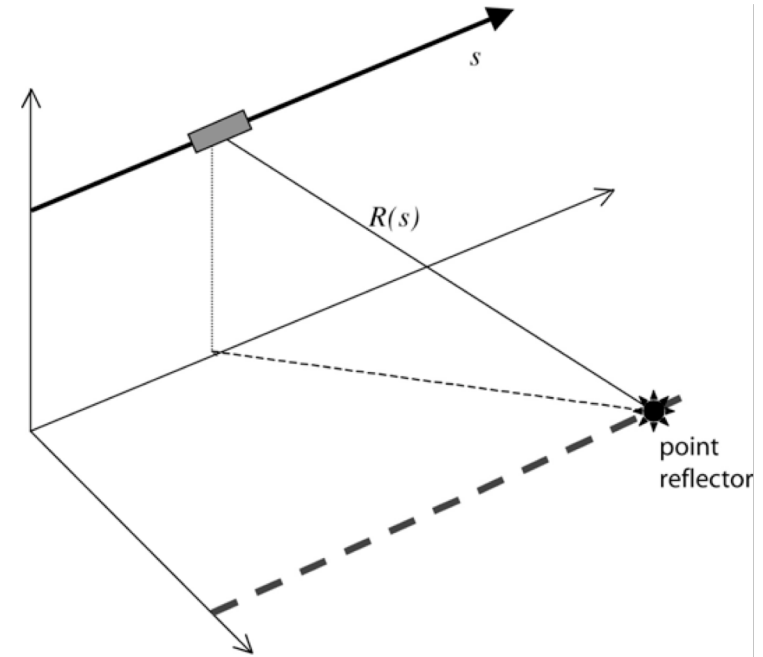


Triggered slip on Southern San Andreas Fault



Need for Precise Orbits

1. proper focus
2. transform from geographic radar coordinates
3. image alignment
4. flattening interferogram



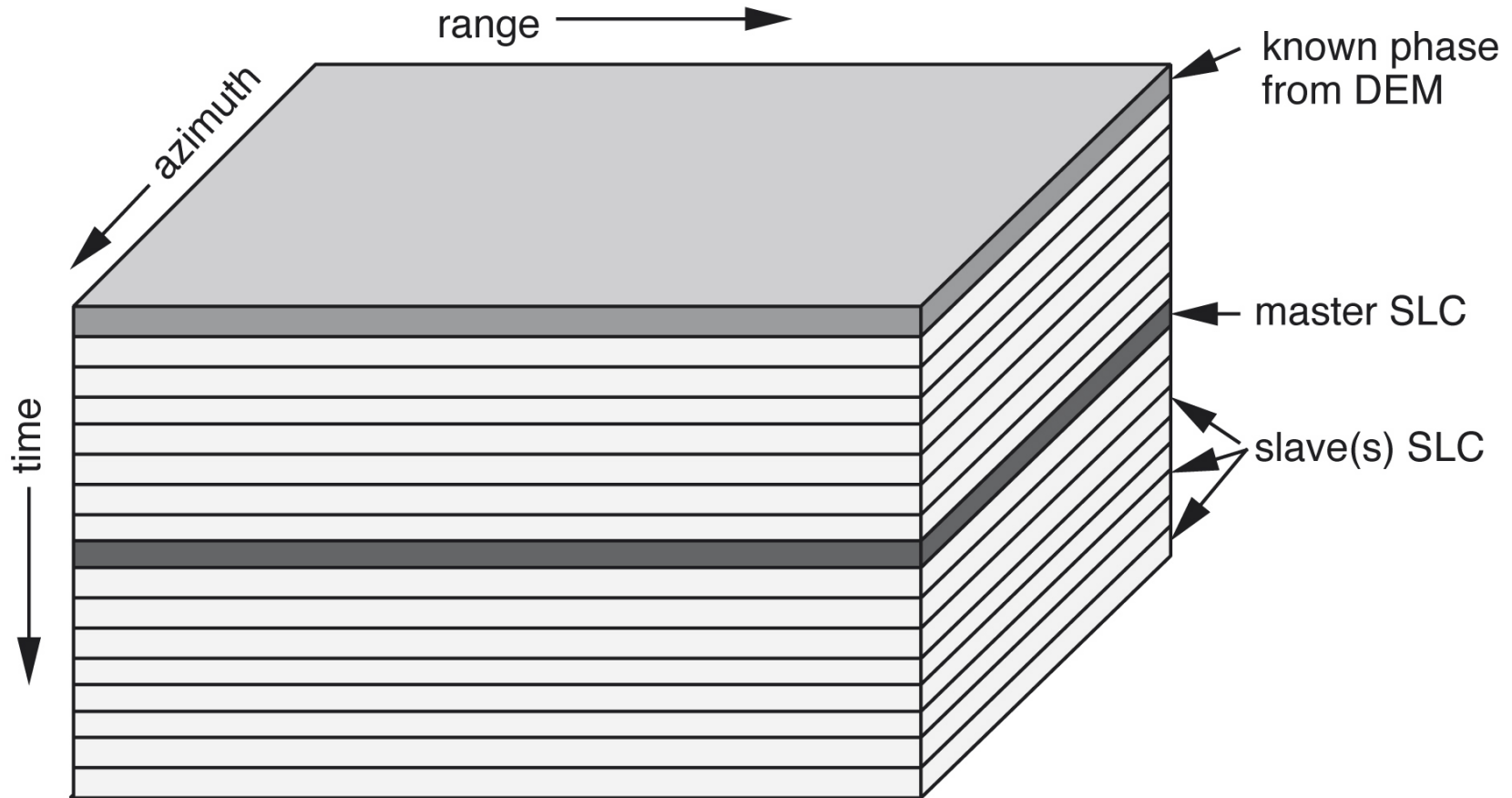
Brute force algorithm given precise orbit subroutine

pick target point

fly satellite along orbit and identify point of closest approach

(This is inefficient but computers are fast so don't waste time coding.)

Batch processing for time series

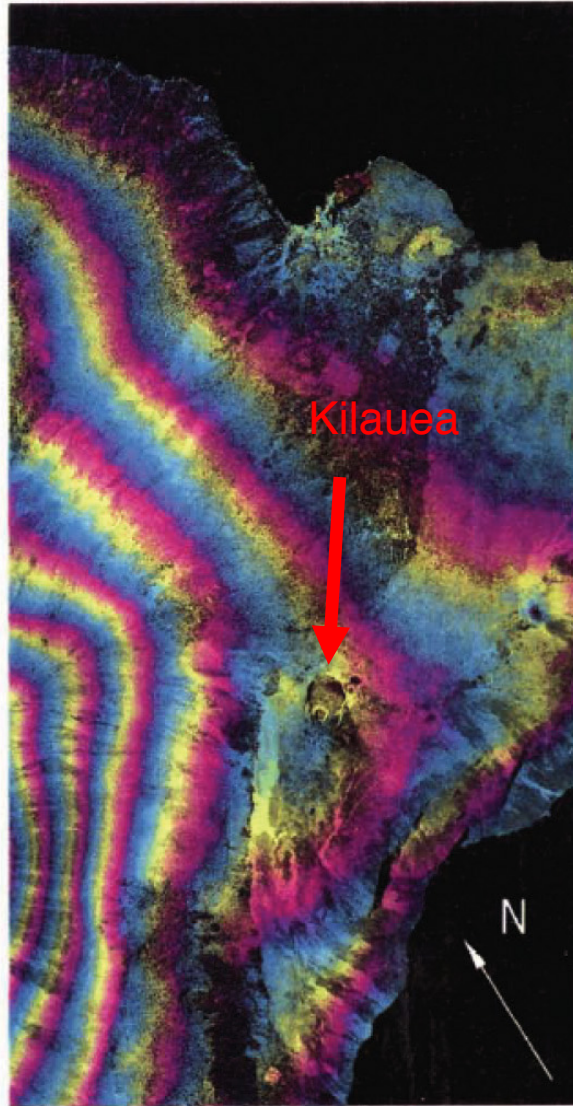


L-band vs. C-band

a) C-Band $\lambda = 5.6 \text{ cm}$



b) L-Band $\lambda = 24 \text{ cm}$



1 Cycle of Interferometric Phase

improved coherence

[Rosen et al., JGR, 1996]

lower fringe rate =
lower range precision?,
easier phase unwrapping

ionospheric delay 16x worse at L-band

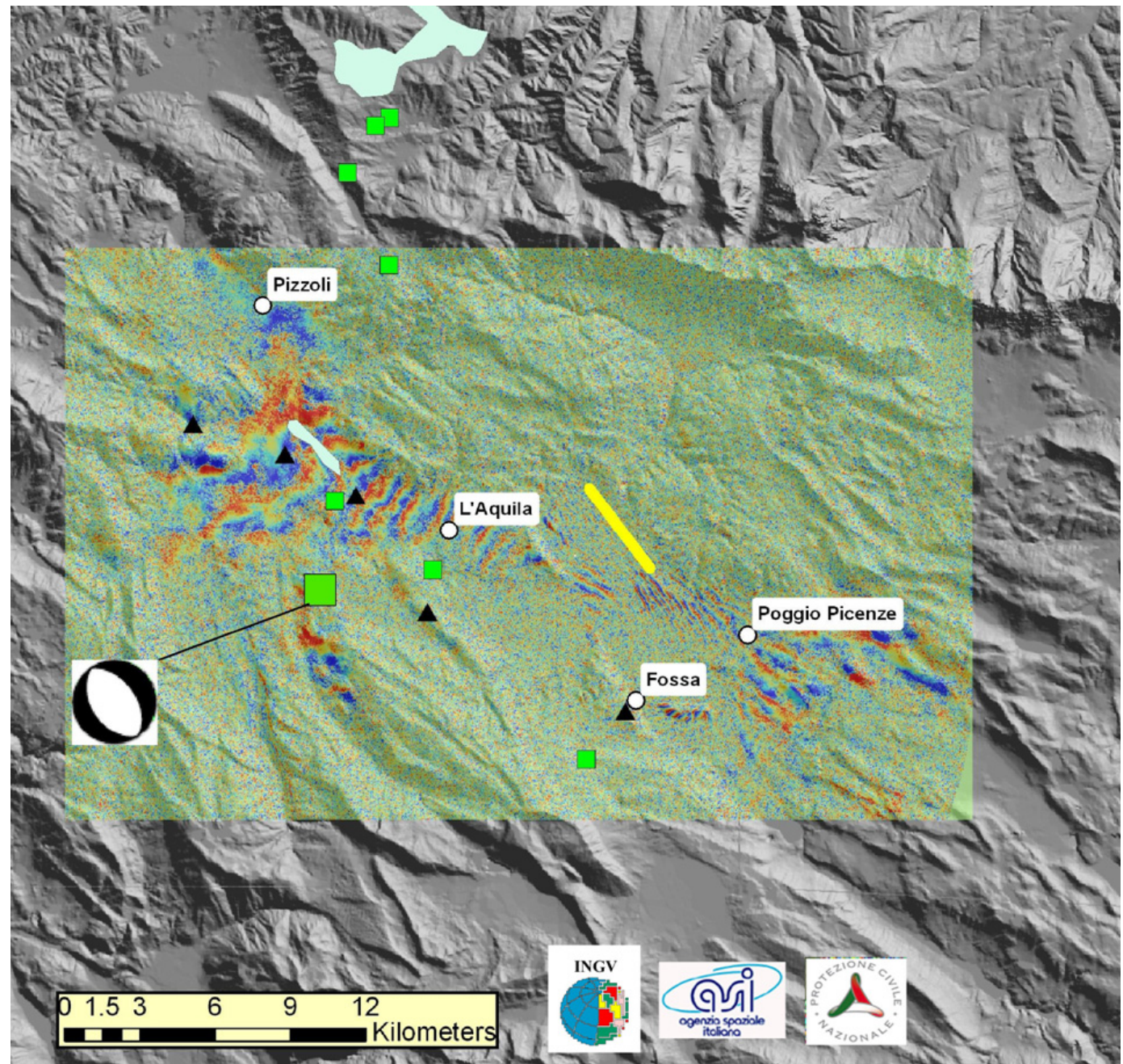
X-band

3 cm
TerraSAR

COSMO-SkyMed

interferogram using data from 19 February 2009 and 9 April 2009. Perpendicular baseline is 480 m, and the satellite's right-looking angle is 37 degrees. The large green square represents the Mw 6.3 main shock, smaller green squares represent the Mw > 5 aftershocks, the yellow line marks the observed co-seismic surface breaks and the black triangles represent GPS stations used for SAR validation.

http://www.esa.int/esaEO/SE_M4PJ9NJTF_index_1.html

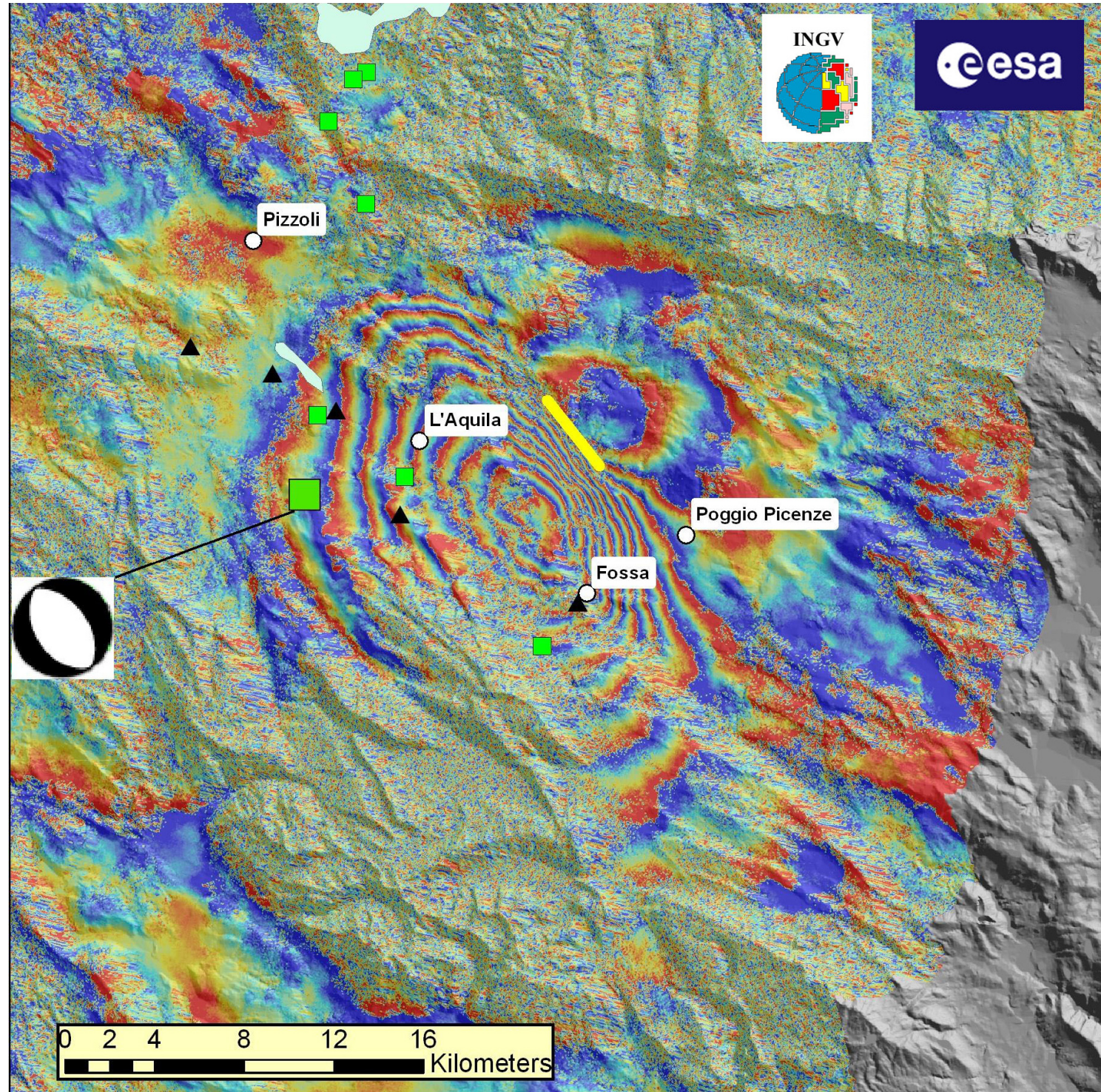


C-band

6 cm
ERS-1/2
Radarsat-1/2
Envisat
Sentinel

Envisat interferogram interpretation by Italy's Istituto Nazionale di Geofisica e Vulcanologia (INGV). The large green square represents the Mw 6.3 main shock, the smaller green squares represent the Mw > 5 aftershocks and the black triangles represent GPS stations used for SAR validation. The yellow line east of L'Aquila shows the location of a ~4 km-long alignment of co-seismic surface breaks observed in the field by INGV researchers. This alignment corresponds to a northwest-southeast strip where the spatial fringe rate seems to exceed the limit for interferometric correlation. This may indicate that the fault dislocation reached, or was very close to, the surface along this line. The observed pattern of ground displacement is in very good agreement with the earthquake source mechanism (the 'beach ball'), confirming that the earthquake source is a normal fault striking 144 degrees (clockwise from north), and dipping to the southwest.

http://www.esa.int/esaEO/SEM4PJ9N_JTF_index_1.html



L-band

- 23 cm
- JERS-1
- ALOS-1/2
- UAVSAR
- NiSAR

ALOS-1

On April 6, 2009 (UTC), magnitude 6.3 earthquake occurred in central Italy. The Japan Aerospace Exploration Agency (JAXA) performed an emergency observation on April 22, 2009 using the Phased Array Type L-band Synthetic Aperture Radar (PALSAR) installed on the Advanced Land Observing Satellite (ALOS) to determine the state of damage caused by the earthquakes. In this report, we conducted differential interferometric SAR (DInSAR) analysis to detect crustal deformation using the data acquired on April 22, 2009 and July 20, 2008

http://www.eorc.jaxa.jp/ALOS/en/img_up/dis_italia_eq_090423.htm

